

# A Pair of Compact Red Galaxies at Redshift 2.38, Immersed in a 100 kpc Scale Ly $\alpha$ Nebula<sup>1</sup>

Paul J. Francis<sup>2 3</sup>, Gerard M. Williger<sup>4</sup>, Nicholas R. Collins<sup>5</sup>, Povilas Palunas<sup>6</sup>, Eliot M. Malumuth<sup>5</sup>, Bruce E. Woodgate<sup>7</sup>, Harry I. Teplitz<sup>4</sup>, Alain Smette<sup>4</sup>, Ralph S. Sutherland<sup>2</sup>, Anthony C. Danks<sup>8</sup>, Robert S. Hill<sup>5</sup>, Donald Lindler<sup>9</sup>, Randy A. Kimble<sup>7</sup>, Sara R. Heap<sup>7</sup>, John B. Hutchings<sup>10</sup>

## ABSTRACT

We present Hubble Space Telescope (HST) and ground-based observations of a pair of galaxies at redshift 2.38, which are collectively known as 2142–4420 B1 (Francis et al. 1996). The two galaxies are both luminous extremely red objects (EROs), separated by 0.8". They are embedded within a 100 kpc scale diffuse Ly $\alpha$  nebula (or blob) of luminosity  $\sim 10^{44}$  erg s<sup>-1</sup>.

The radial profiles and colors of both red objects are most naturally explained if they are young elliptical galaxies: the most distant yet found. It is not, however, possible to rule out a model in which they are abnormally compact, extremely dusty starbursting disk galaxies. If they are elliptical galaxies, their stellar populations have inferred masses of  $\sim 10^{11} M_{\odot}$  and ages of  $\sim 7 \times 10^8$  years. Both

---

<sup>1</sup>Based upon observations with the Anglo-Australian Telescope, the Cerro Tololo Blanco Telescope, observations taken with the ESO New Technology Telescope (NTT) at the La Silla Observatory under program-ID No.63.0-0291(A), and observations taken with the NASA/ESA Hubble Space Telescope, obtained at the Space Telescope Science Institute, which is operated by the Association of Universities for Research in Astronomy, Inc., under NASA contract No. NASS-26555

<sup>2</sup>Research School of Astronomy and Astrophysics, The Australian National University, Canberra, ACT 0200, Australia

<sup>3</sup>Joint appointment with the Department of Physics, Faculty of Science.

<sup>4</sup>NOAO, Code 681, NASA Goddard Space Flight Center, Greenbelt, MD 20771

<sup>5</sup>Raytheon ITSS, Code 681, Goddard Space Flight Center, Greenbelt, MD 20771

<sup>6</sup>Catholic University of America, Goddard Space Flight Center, Code 681, Greenbelt, MD 20771

<sup>7</sup>NASA Goddard Space Flight Center, Code 681, Greenbelt, MD 20771

<sup>8</sup>Raytheon RPSC, Code 681, Goddard Space Flight Center, Greenbelt, MD 20771

<sup>9</sup>Advanced Computer Concepts, Inc., Goddard Space Flight Center, Code 681, Greenbelt, MD 20771

<sup>10</sup>Dominion Astrophysical Observatory, Victoria, BC V8X 4M6, Canada

galaxies have color gradients: their centers are significantly bluer than their outer regions. The surface brightness of both galaxies is roughly an order of magnitude greater than would be predicted by the Kormendy relation. A chain of diffuse star formation extending  $1''$  from the galaxies may be evidence that they are interacting or merging.

The Ly $\alpha$  nebula surrounding the galaxies shows apparent velocity substructure of amplitude  $\sim 700 \text{ km s}^{-1}$ . We propose that the Ly $\alpha$  emission from this nebula may be produced by fast shocks, powered either by a galactic superwind or by the release of gravitational potential energy.

*Subject headings:* galaxies: formation — galaxies: evolution — galaxies: interaction — galaxies: individual (2142–4420 B1)

## 1. Introduction

Two of the most enigmatic types of high redshift galaxy are the extremely red objects (EROs, eg. Hu & Ridgway 1994; Thompson et al. 1999), and the Ly $\alpha$  blobs (eg. Lowenthal et al. 1991; Francis et al. 1996; Keel et al. 1999; Steidel et al. 2000; Roche, Lowenthal & Woodgate 2000; Kobulnicky & Koo 2000).

EROs are defined as having extremely red observed-frame optical/near-IR colors, and may be dusty starburst galaxies or AGN (eg. Smail et al. 1999; Hughes et al. 1998), or spheroidal galaxies (eg. Cimatti et al. 1999; Dunlop et al. 1996; Soifer et al. 1999; Moriondo, Cimatti & Daddi 2000).

The Ly $\alpha$  blobs are characterized by 100 kpc scale low surface brightness Ly $\alpha$  nebulae, with total Ly $\alpha$  luminosities  $> 10^{43} \text{ erg s}^{-1}$ . All Ly $\alpha$  blobs identified to date appear to lie in proto-cluster environments. It has been proposed that these blobs are a form of AGN, that they are associated with cooling flows (Steidel et al. 2000; Haiman, Spaans & Quataert 2000) or that they are generated by galaxy superwinds (Taniguchi & Shioya 2000).

Can a galaxy be both an ERO and a Ly $\alpha$  blob? Many high redshift radio galaxies contain ERO nuclei embedded within dense gaseous regions, which are often associated with extended diffuse Ly $\alpha$  emission (eg. McCarthy 1993; Pentericci et al. 1997; Ivison et al. 2000; Carilli et al. 1997; Binette et al. 2000; Bicknell et al. 2000).

In this paper we present a detailed study of a *radio quiet* Ly $\alpha$  blob that contains two compact EROs. Francis et al. (1996) identified 2142–4420 B1, which is a luminous Ly $\alpha$  and C IV emitting source at redshift  $z = 2.38$ . The enormous Ly $\alpha$  luminosity of this source

comes from an extended  $\sim 100$  kpc low surface brightness nebula. Ground-based near-IR observations showed an unresolved, luminous, extremely red source lying within this blob. The whole system appears to lie within a cluster of Lyman-limit QSO absorption-line systems (Francis, Wilson & Woodgate 2000). The optical properties of this source closely resemble those of many high redshift radio galaxies, but Francis et al. (1996) obtained an upper limit on its radio flux of 0.27 mJy at 1344 and 2378 MHz.

We describe our observations in Section 2, and show the results in Section 3. We then discuss the nature of the ERO (Section 4) and of the Ly $\alpha$  blob surrounding it (Section 5). In Section 6 we conclude that this object is probably a pair of young merging elliptical galaxies, though a compact dusty starburst model is hard to completely exclude. We further conclude that the Ly $\alpha$  nebula surrounding them is either photoionized by an AGN or shock excited by the energy of gravitational infall or of a superwind.

We assume a flat universe with  $H_0 = 70\text{km s}^{-1}\text{Mpc}^{-1}$ ,  $\Omega_m = 0.3$  and  $\Omega_\Lambda = 0.7$ . At  $z = 2.38$ , given this cosmology and redshift, one arcsecond corresponds to 8.0 proper Kpc, and the luminosity distance is 18.8 Gpc.

## 2. Observations

Our previous observations of this object can be found in Francis & Hewett (1993); Francis et al. (1996); Francis, Woodgate & Danks (1997) and Francis, Wilson & Woodgate (2000). The observation log is in Table 1. HST imaging was used to determine the morphology and colors of B1. Ground-based imaging measured its integrated colors and diffuse Ly $\alpha$  emission. Slitless spectroscopy and Fabry-Perot imaging was used to constrain the velocity structure.

In addition to our own observations, we searched the ROSAT All Sky Survey (Voges et al. 1999) for data on this object. There is only a 308 sec exposure toward the field, giving a 90% upper limit X-ray count rate of 0.0075 counts  $\text{sec}^{-1}$ . Assuming a Galactic column density of  $2.65 \times 10^{20} \text{ cm}^{-2}$  along this line of sight (which is the weighted mean of the four nearest 21 cm measurements) and a power law spectrum with an energy index of 1.0, we obtain a flux  $f_E < 2.6 \times 10^{-5} \text{ E}^{-2} \text{ photons cm}^{-2} \text{ sec}^{-1} \text{ keV}^{-1}$  where E is the energy in keV.

### 2.1. WFPC2 Imaging

The cluster region was observed for 38 orbits with the Wide Field and Planetary Camera II (WFPC2, Trauger et al. 1994) on the Hubble Space Telescope. Galaxy B1 was placed on the WF3 chip. Exposures were dithered on a sub-pixel grid, to allow reconstruction of a

Table 1. Observations

Instrument	Filter	Rest-frame $z = 2.38$ wavelength (nm)	Exposure (s)	Date	Notes
HST/WFPC2	F410M	$121 \pm 2.1$	67200	1999 Aug 27—Sep 8	
HST/WFPC2	F450W	$131 \pm 13$	19400	1999 Aug 31—Sep 2	
HST/WFPC2	F702W	$207 \pm 21$	14400	1999 Aug 23	
HST/NICMOS	F110W	$325 \pm 87$	5120	1998 Jun 27	
HST/NICMOS	F160W	$471 \pm 54$	10112	1998 Oct 30	a
HST/NICMOS	F164N	$487 \pm 2.5$	10236	1997 Oct 30	a
HST/STIS	Clear		3120	1998 Oct 25—27	b
HST/STIS	G430L		17000	1998 Oct 25—27	c
NTT/SOFI	<i>J</i>	$369 \pm 43$	3540	1999 Aug 16	
NTT/SOFI	<i>H</i>	$489 \pm 44$	4740	1999 Aug 16	
NTT/SOFI	<i>K<sub>s</sub></i>	$640 \pm 40$	3480	1999 Aug 16	
CTIO/Mosaic	4107Å	$121.5 \pm 0.8$	18000	1999 Aug 7	
CTIO/Mosaic	<i>U</i>	$108 \pm 10$	9000	1999 Aug 8	
CTIO/Mosaic	<i>B</i>	$130 \pm 14$	7200	1999 Aug 7—8	
CTIO/Mosaic	<i>V</i>	$163 \pm 13$	7800	1999 Aug 7—8	
CTIO/Mosaic	<i>R</i>	$207 \pm 32$	2400	1999 Aug 8	
CTIO/Mosaic	<i>I</i>	$260 \pm 35$	4800	1999 Aug 8	
AAT/TTF	4110Å	$121.6 \pm 0.6$	5400	1999 Sep 11	d
AAT/TTF	4114Å?	$121.7 \pm 0.6$	5400	1999 Sep 11	d
AAT/TTF	4118Å	$4121.8 \pm 0.6$	9000	1999 Sep 12	d

<sup>a</sup>Not taken during a NIC3 focus campaign. Image quality degraded, and image partially vignetted

<sup>b</sup>Taken to allow registration of the slitless spectroscopy

<sup>c</sup>Slitless spectroscopy

<sup>d</sup>Wavelength calibration uncertain

better sampled image. Broad-band images were obtained through the F450W and F702W filters. Relatively narrow-band images were taken through the F410M filter, which matches the wavelength of Ly $\alpha$  at the cluster wavelength. The F410M images suffer from a very low surface brightness, time-varying mottling. We hypothesise that this is caused by scattered Earth-light.

The images were pipeline processed, then cosmic rays were removed and the frames co-added using the drizzle algorithm (Fruchter & Hook 1998) to minimise undersampling.

## 2.2. STIS Slitless Spectroscopy

The Space Telescope Imaging Spectrograph (STIS, Woodgate et al. 1998) observations (pairs of slitless spectra and images) were taken at two different orientation angles separated by 11.5 deg, in an attempt to separate slitless spectra from objects aligned along the same row for a given angle. For both the direct clear-aperture and the dispersed images, the CCD was binned  $2 \times 2$ , producing a plate scale of 0.1 arcsec/pixel, and spectral resolution  $\sim 11$  Å for point sources. There were 20 exposures each for the direct and dispersed images, with dithering of  $\sim 1.4$  arcsec between each exposure in order to minimize the effects of cosmic rays and hot pixels. The direct and dispersed images were combined using the STIS GTO team software CALSTIS (Lindler 1998; Gardner et al. 1998). The spectra were extracted using both the STIS\_EXTRACT (Chen, Lanzetta & Pascarelle 1999) and SLWIDGET (Lindler 2000) software. Results from both were consistent.

## 2.3. NICMOS Imaging

The Near Infrared Camera and Multi Object Spectrometer (NICMOS, Thompson et al. 1998) observations were made with Camera 3, through the F110W, F160W and F164N filters. All exposures were dithered for each filter over 4 (or 8 in the case of F160W) positions spanning a  $2 \times 2$  arcsec box, to minimize the effects of bad pixels. The F160W and F164N observations are affected by vignetting from the field offset mirror, and were taken before the focus became optimal. The NICMOS data were reduced using the same methods as for SOFI (Section 2.4). The data were also reduced using NICRED (McLeod 1997); there is little difference between final images reduced by the two methods. A comparison of broadband SOFI and NICMOS data show the photometry to be consistent between the two, with the exception of a vignetted band along one end of the chip in the F160W and F164W images.

## 2.4. NTT Imaging

Near-IR photometry was obtained with the SOFI camera on the ESO New Technology Telescope (NTT, Lidman, Cuby & Vanzi 2000). Conditions were photometric, but seeing was  $\sim 1.1''$  and the telescope was subject to considerable wind shake. The data were reduced using a modified version of IRAF<sup>11</sup> scripts written by Peter McGregor. NICMOS standards (Persson et al. 1998) were used.

## 2.5. Cerro Tololo 4m Imaging

We obtained broad- and narrow-band ( $\text{Ly}\alpha$ ) imaging of this field with the MOSAIC camera (Muller et al. 1998), at the prime focus of the Cerro Tololo Inter-American Observatory (CTIO) 4m Blanco Telescope. The narrow-band images were taken through a specially purchased filter, which working in the f/2.8 beam has a bandpass of  $54\text{\AA}$ , centered at  $4107\text{\AA}$ . Conditions were mostly photometric, with seeing  $\sim 1.2''$ .

## 2.6. Anglo-Australian Telescope Narrow-band Imaging and Spectroscopy

Our Anglo-Australian Telescope imaging was obtained with the Taurus Tunable Filter (TTF, Bland-Hawthorn & Heath-Jones 1998), which is a Fabry-Perot etalon system. Conditions were photometric on the first night, and the typical image quality was  $\sim 1.6''$ . A MIT-Lincoln Labs CCD was used behind the TTF.

The TTF was used with a full-width at half maximum (FWHM) spectral resolution of between  $3.35$  and  $4.4\text{\AA}$ . Images were obtained at central wavelengths of  $4110\text{\AA}$ ,  $4114\text{\AA}$ , and  $4118\text{\AA}$ .

An electronics fault was subsequently found to induce significant wavelength drifts on timescales of a few hours. The  $4110$  and  $4118\text{\AA}$  observations were taken within four hours of a calibration, but the  $4114\text{\AA}$  observations were taken between four and eight hours after the calibration. Thus the wavelength calibration of all three images are somewhat uncertain, particularly that of the  $4114\text{\AA}$  image.

We obtained a long-slit spectrum of B1 with the Low Dispersion Survey Spectrograph

---

<sup>11</sup>IRAF is distributed by the National Optical Astronomy Observatories, which is operated by the Association of Universities for Research in Astronomy, Inc. (AURA) under cooperative agreement with the National Science Foundation.

(LDSS, Wynne & Worswick 1988). These observations are described in Francis, Woodgate & Danks (1997)

### 3. Results

Our images of B1 are shown in Figures 1 & 2. The appearance of B1 varies dramatically as a function of wavelength and resolution. In the observed-frame red and near-IR, it breaks up into two compact components: B1a and B1b (Fig 2), separated by  $0.8''$ . In this respect it is similar to another strong, high redshift Ly $\alpha$  source, the Coup-Fouéré galaxy (Roche, Lowenthal & Woodgate 2000). A third continuum source, B1c, appears as chain of diffuse knots extending about  $1''$  to the south from B1a and B1b.

In Ly $\alpha$ , the picture is different again. When viewed with WFPC2, we see a knot of Ly $\alpha$  emission from B1b, but no emission from B1a. Diffuse patches of low surface brightness Ly $\alpha$  emission are found  $\sim 1''$  to the south and north-east of B1b. The ground-based CTIO image has much greater sensitivity to low surface brightness Ly $\alpha$  emission, and confirms that it extends at least  $10''$  north-east of B1a and B1b, as reported by Francis et al. (1996) and Francis, Woodgate & Danks (1997). The non-detection of this emission in the WFPC2 image indicates that it is truly diffuse, and not coming from a series of compact sources separated by less than the ground-based resolution limit (as was the case for the Ly $\alpha$  nebula observed by Pascarelle et al. (1996)).

The Ly $\alpha$  contribution to the blue continuum images, and the blue continuum contribution to the narrow-band Ly $\alpha$  images, were removed. B1 has a total Ly $\alpha$  flux of about  $1.5 \times 10^{-15} \text{erg cm}^{-2} \text{s}^{-1}$ : a more exact number is hard to calculate as the diffuse flux fades gradually into the sky (this number is for a rectangular aperture  $10''$  long and  $5''$  wide, aligned along the major axis of the Ly $\alpha$  flux). B1b has a Ly $\alpha$  flux of  $\sim 2.0 \times 10^{-16} \text{erg cm}^{-2} \text{s}^{-1}$ , which is only  $\sim 13\%$  of the total. The remaining flux is diffuse: the average Ly $\alpha$  surface brightness of the region within  $2''$  of B1b is  $\sim 4 \times 10^{-17} \text{erg cm}^{-2} \text{s}^{-1} \text{arcsec}^{-2}$ .  $4''$  further east, the average surface brightness drops to  $\sim 10^{-17} \text{erg cm}^{-2} \text{s}^{-1} \text{arcsec}^{-2}$ .

#### 3.1. Fluxes

Continuum fluxes (Table 3) were calculated for the three components of B1. Small circular apertures were used:  $0.3''$  in radius for B1a and B1b, and  $0.65''$  for B1c. These small apertures will miss much of the flux of these components, but were chosen to avoid contamination from the other components. No aperture corrections were attempted. A total

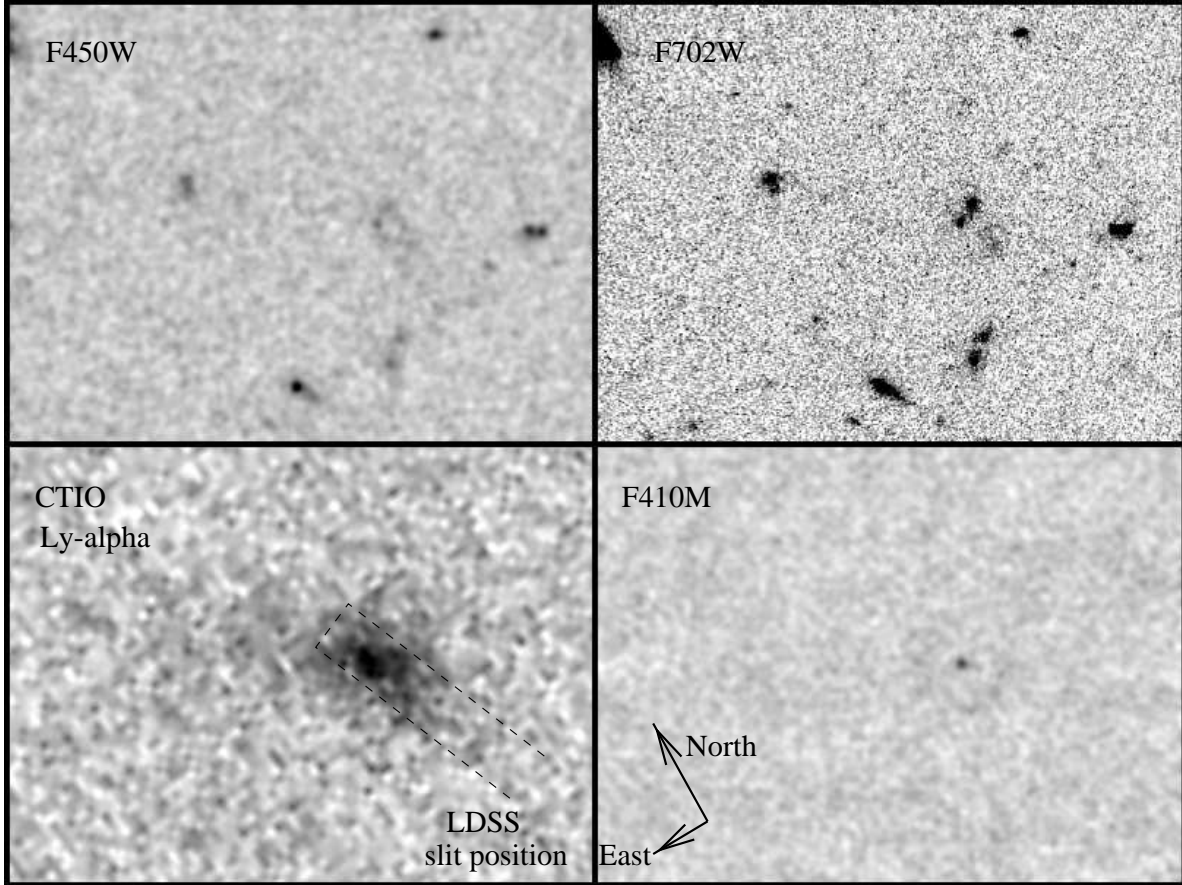


Fig. 1.— Images of a  $20''$  by  $15''$  region around the centre of B1. The bottom left image is the CTIO Ly $\alpha$  image. The F410M and F450W images have been smoothed with a Gaussian of  $\sigma = 2$  pixels ( $0.1''$ ). The CTIO image has been rotated to match the orientation of the WFPC2 images. The continuum has been removed from the Ly $\alpha$  images, and the Ly $\alpha$  component has been removed from the F450W image.



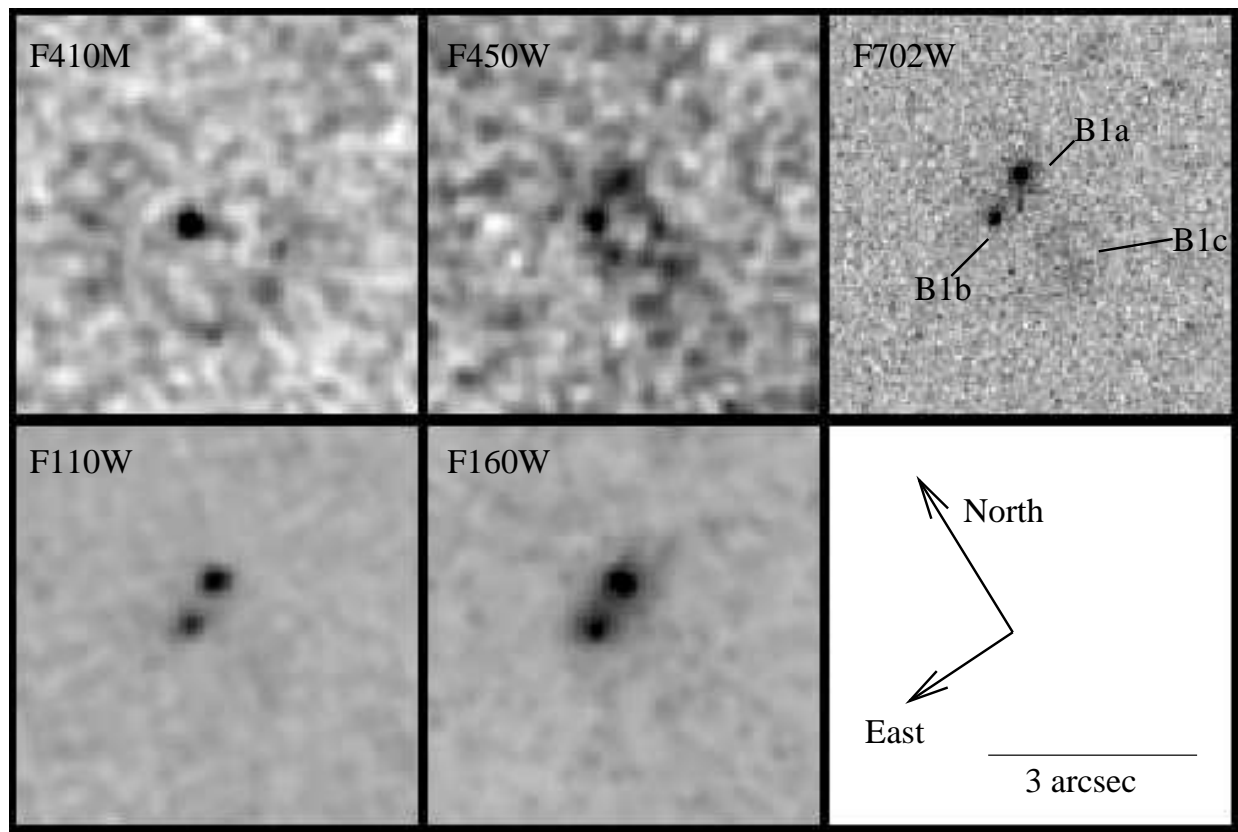


Fig. 2.— Close-up of the continuum sources in B1. The F410M and F450W images have been smoothed with a Gaussian of  $\sigma = 2$  pixels ( $0.1''$ ). The NICMOS images have been rotated to match the orientation of the WFPC2 images. The orientation matches that of Fig 1.

flux for B1 was also measured, using a  $2''$  radius aperture.

Error estimates were made using apertures placed randomly on sky regions. A copy of the image was made with all the sources detected by the SExtractor (Bertin & Arnouts 1996) package masked out. We randomly placed 1000 apertures of identical radius on the image. Any aperture that fell on a masked region was rejected, and the procedure continued until 1000 clean measurements had been obtained. The standard deviation of these measurements is our sky error estimate. A Poisson noise model was combined with the sky error estimate to calculate object flux errors. The  $\text{Ly}\alpha$  contribution to the F450W flux has been removed, but the probable emission-line contributions to F110W, F160W and  $K_s$  have not been removed: these contributions are discussed in Section 3.1.1. Finally, the fluxes were corrected for the local Milky Way extinction ( $E(B - V) = 0.019$ ), as estimated by Schlegel, Finkbeiner & Davis (1998). The extinction curve of Cardelli, Clayton & Mathis (1989) was used.

Integrated near-IR magnitudes for B1 were measured from the NTT image, using SExtractor with  $4.2''$  radius circular apertures. We measure  $J = 21.71 \pm 0.12$ ,  $H = 20.31 \pm 0.08$  and  $K_s = 19.47 \pm 0.10$ .

The measured coordinates of the components of B1 are shown in Table 2.

### 3.1.1. Emission-line Contamination

The near-IR filters are subject to possible emission-line contamination at this redshift,  $z=2.38$ . [O II] ( $3727 \text{ \AA}$ ) is redshifted into the  $J$ -band,  $\text{H}\beta$  and the [O III] ( $4959$  and  $5007 \text{ \AA}$ ) doublet are shifted into the  $H$ -band, and  $\text{H}\alpha$  and [N II] ( $6583 \text{ \AA}$ ) are shifted into the  $K$  band. These lines could in principle be very strong (eg. Eales et al. 1993). In this section, we estimate their strength, and conclude that it is probably small.

As described in Francis et al. (1996), we imaged the field with a narrow-band filter of

Table 2. B1 Component Coordinates

Component	Coordinates (J2000)
B1a	21:42:27.45–44:20:28.69
B1b	21:42:27.51–44:20:28.99
B1c	21:42:27.46–44:20:30.2

wavelength coverage  $2.238 \pm 0.024 \mu\text{m}$ , which includes both  $\text{H}\alpha$  and  $[\text{N II}]$ . Using a  $5''$  radius aperture, we determine that these lines contribute  $21 \pm 10\%$  of the integrated  $K_s$  flux of B1. The F164N NICMOS image covers the wavelength of redshifted  $\text{H}\beta$ . No significant narrow-band excess was detected: we can place a  $3\sigma$  upper limit on the fraction of the integrated  $H$ -band light coming from  $\text{H}\beta$  in B1 of  $3\%$ .

We have no direct measurements of the other line fluxes, so we estimate their importance by making assumptions about their ratios with measured Balmer lines. Typical line ratios were taken from Osterbrock & Martel (1993), Kennicutt (1992) and Teplitz et al. (2000), for a variety of assumed chemical compositions and ionization sources, and including both narrow- and broad-line AGN ratios.

We conclude that line emission probably contributes only  $\sim 20\%$  at most of the total continuum flux of B1 in  $H$  and  $K_s$ . In  $J$ , the contribution is probably  $\sim 5\%$ . Furthermore, only about  $10\%$  of the line flux will likely come from within the photometric aperture of B1b, and  $\sim 20\%$  from within the aperture of the B1c. The remainder of the optical emission lines will come from the region of the diffuse blob. As B1a shows no  $\text{Ly}\alpha$  emission, its rest-frame optical line flux is also probably small.

The line corrections will thus probably be minimal. We have not, therefore, applied any emission-line corrections to the near-IR fluxes.

### 3.2. Velocity Structure

The  $\text{Ly}\alpha$  line is generally extremely optically thick and often strongly self absorbed, making it a very unreliable tracer of dynamics. It is, however, the only sufficiently strong line available to us, and can be used to place some limits on the dynamics of the  $\text{Ly}\alpha$  nebula surrounding B1.

The velocity dispersion of the gas around B1 (measured at the peak of the surface brightness, as seen in ground-based images) is  $\sim 600 \text{km s}^{-1}$  (Francis et al. 1996).  $\text{Ly}\alpha$  is redshifted with respect to C IV, indicating probable self absorption. The deep multislit spectroscopy of Francis, Woodgate & Danks (1997) marginally spatially resolves this emission along the slitlet. Fig 3 shows the spectra extracted from different CCD columns: notice the extra component at  $+1000 \text{km s}^{-1}$  in the southernmost spectrum (and another possible component at  $-1000 \text{km s}^{-1}$ ).

The diffuse  $\text{Ly}\alpha$  structure differs significantly between the three TTF images. This confirms the existence of multiple velocity components separated by  $\sim 700 \text{km s}^{-1}$ . It is

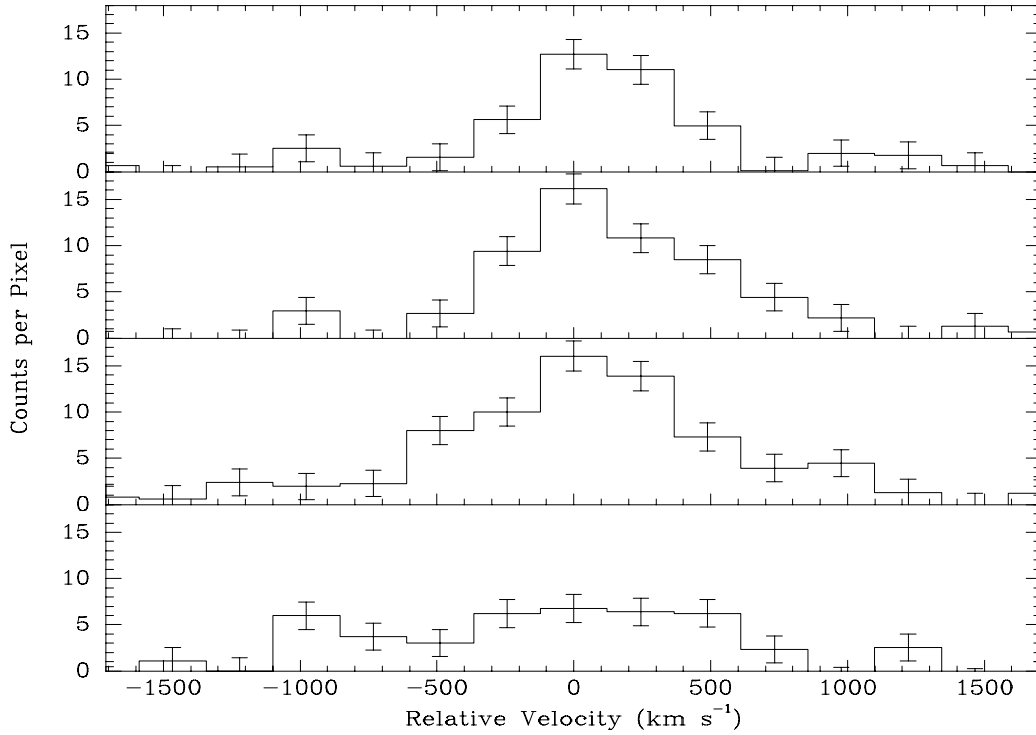


Fig. 3.— Longslit Ly $\alpha$  spectra of B1. The slit orientation is shown in Fig 1. The four panels are the spectra extracted from the four adjacent CCD columns along which Ly $\alpha$  was detected: the top panel is the northernmost. Each pixel is  $0.83''$  wide: the seeing was  $1.2''$ , so the spectra are not independent. Positive velocities represent redshifts. Spectral resolution is  $700\text{km s}^{-1}$ , so the line core is not resolved in the top three panels. The velocity zero point is arbitrary.

hard to say more, given the uncertainty in the wavelength calibration of the TTF data (Section 2.6).

The STIS spectrum detected the Ly $\alpha$  flux from B1b. A flux of  $1.57 \pm 0.40 \times 10^{-16} \text{erg cm}^{-2} \text{s}^{-1}$  was measured, consistent with the value derived from the WFPC2 imaging. The line was not significantly spectrally resolved; an upper limit on the velocity dispersion of  $\sim 1400 \text{km s}^{-1}$  can be placed.

## 4. The Continuum

### 4.1. The Colors

The spectral energy distributions (SEDs) of the three components of B1 are shown in Fig 4. B1a and B1b are quite red, while the SED of B1c is very blue. B1c’s colors are similar to those of Lyman-break galaxies (eg. Steidel et al. 1996). A power-law fit to its colors gives a slope of the form  $F_\lambda \propto \lambda^{-1.34}$ , which is close to the median slope of Lyman break galaxies (1.5, Adelberger & Steidel 2000).

Our NTT photometry demonstrates that while B1 is red at wavelengths shortward of  $H$ , it has a relatively blue  $H - K_s$  color. This confirms the result of Francis et al. (1996). B1’s SED thus peaks in the  $H$ -band. As we discussed in Section 3.1.1, this is unlikely to be an artifact of emission-line contamination.

#### 4.1.1. Modelling

We modelled the SEDs of B1 using the 1997 version of the spectral synthesis models of Bruzual & Charlot (1993). Models both with continuous uniform star formation and models in which all the stars were formed in an instantaneous burst (a simple stellar population) were used. All models had Salpeter stellar initial mass functions, with no mass cut-off. Dust was modelled using the empirical absorption curves of Calzetti, Kinney & Storchi-Bergmann (1994). Our predicted colors are compared with the observations in Figures 5 and 6.

The red components, B1a and B1b, can be fit by two models:

- An unreddened burst model of age  $750 \pm 150 \text{ Myr}$  ( $1\sigma$  limits) and stellar mass  $\sim 8 \times 10^{10} M_\odot$ . This naturally fits the  $H$ -band peak (Fig 6) and the photometry from  $F702W$  thru  $K_s$ . It greatly underpredicts the observed  $F450W$  flux of B1a. We do not

Table 3. B1 Component Observed Flux Densities

Filter	Flux ( $\times 10^{20} \text{erg cm}^{-2} \text{s}^{-1} \text{\AA}^{-1}$ )			
	B1 (total)	B1a	B1b	B1c
F450W ( <i>B</i> )	$70.2 \pm 12.4$	$11.2 \pm 1.3$	$< 7.26^{\text{a}}$	$25.7 \pm 3.4$
F702W ( <i>R</i> )	$64.2 \pm 5.1$	$12.3 \pm 0.8$	$10.2 \pm 1.0$	$15.3 \pm 2.2$
F110W ( <i>J</i> )	$47.8 \pm 13.6$	$15.2 \pm 0.8$	$11.5 \pm 0.8$	$< 8.35^{\text{a}}$
F160W ( <i>H</i> )	$120.2 \pm 16.4$	$25.7 \pm 0.9$	$21.3 \pm 0.9$	$7.6 \pm 1.2$

<sup>a</sup> $3\sigma$  upper limit

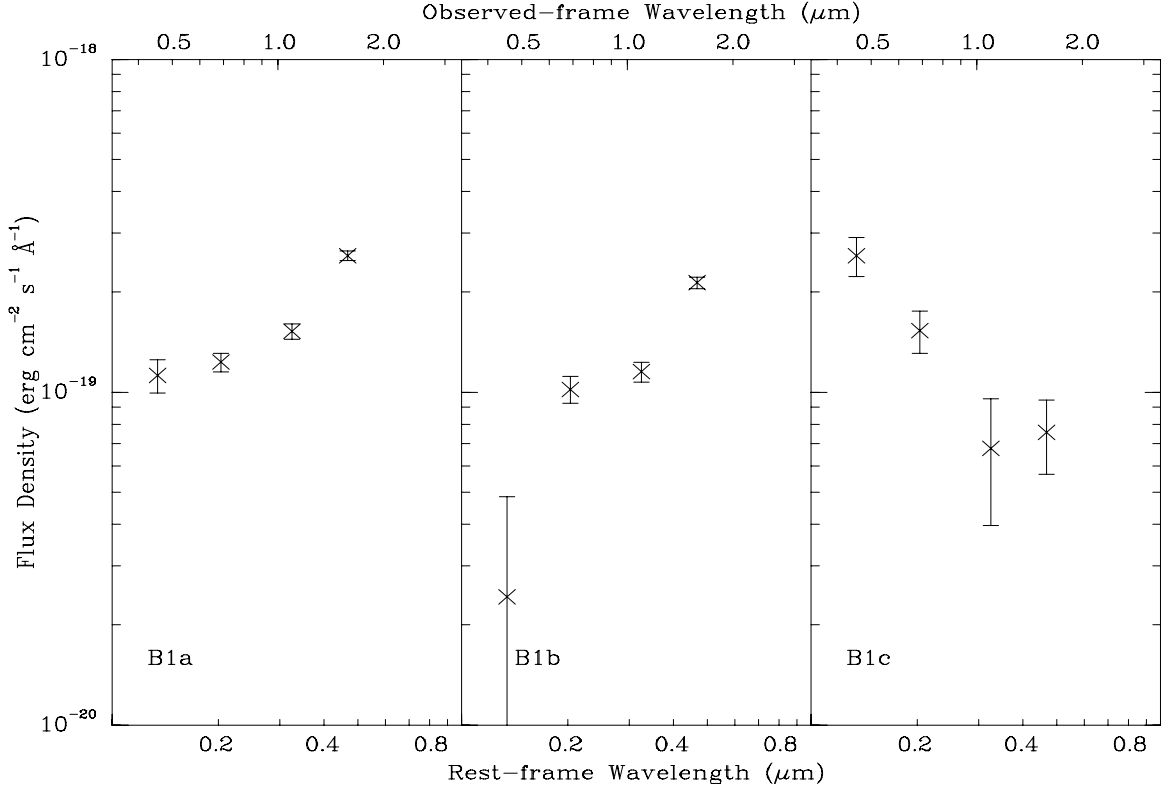


Fig. 4.— The spectral energy distributions of the three components of B1. Ly $\alpha$  emission has been subtracted from the bluest point.

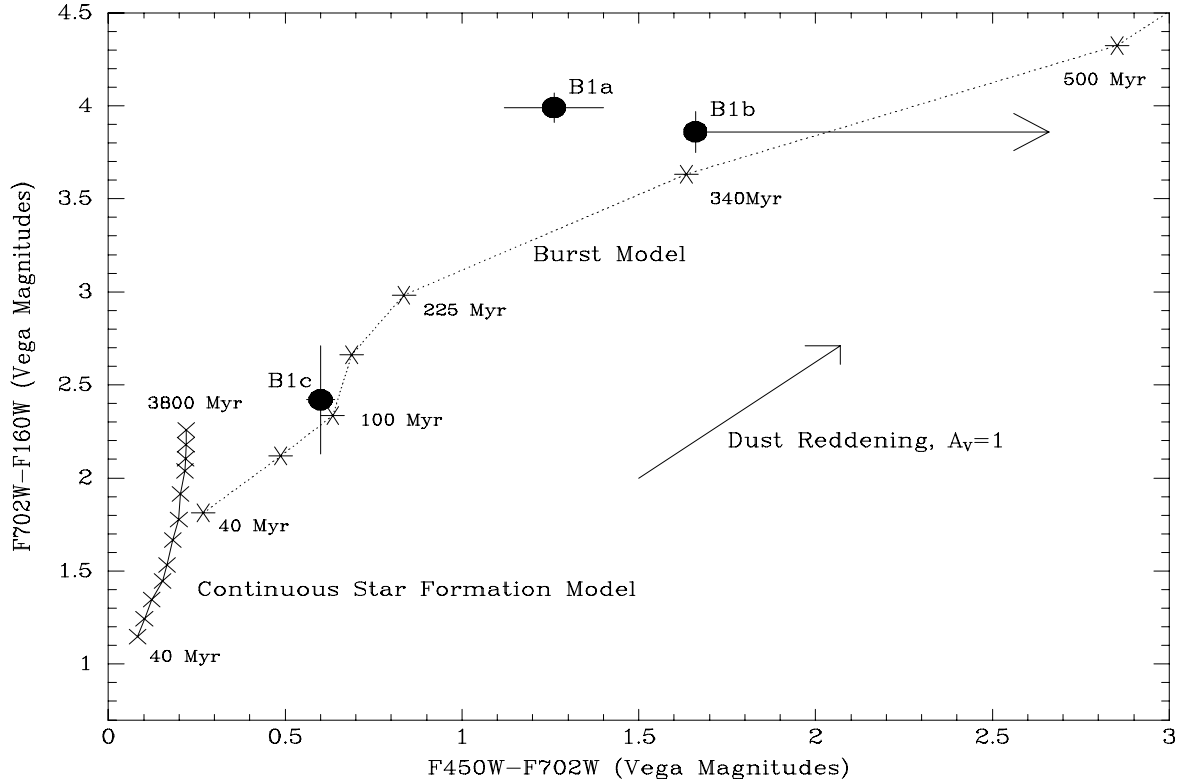


Fig. 5.— The F450W–F702W and F702W–F160W colors of the three components of B1. Both the continuous star formation models (crosses) and the instantaneous burst models (asterisks) have been computed for twelve different ages of the stellar population. From left to right, the model ages are 40, 60, 100, 150, 225, 340, 500, 750, 1125, 1700, 2500 and 3800 Myr. The change in colors caused by dust with a rest-frame  $V$ -band extinction  $A_v$  of one magnitude is shown.

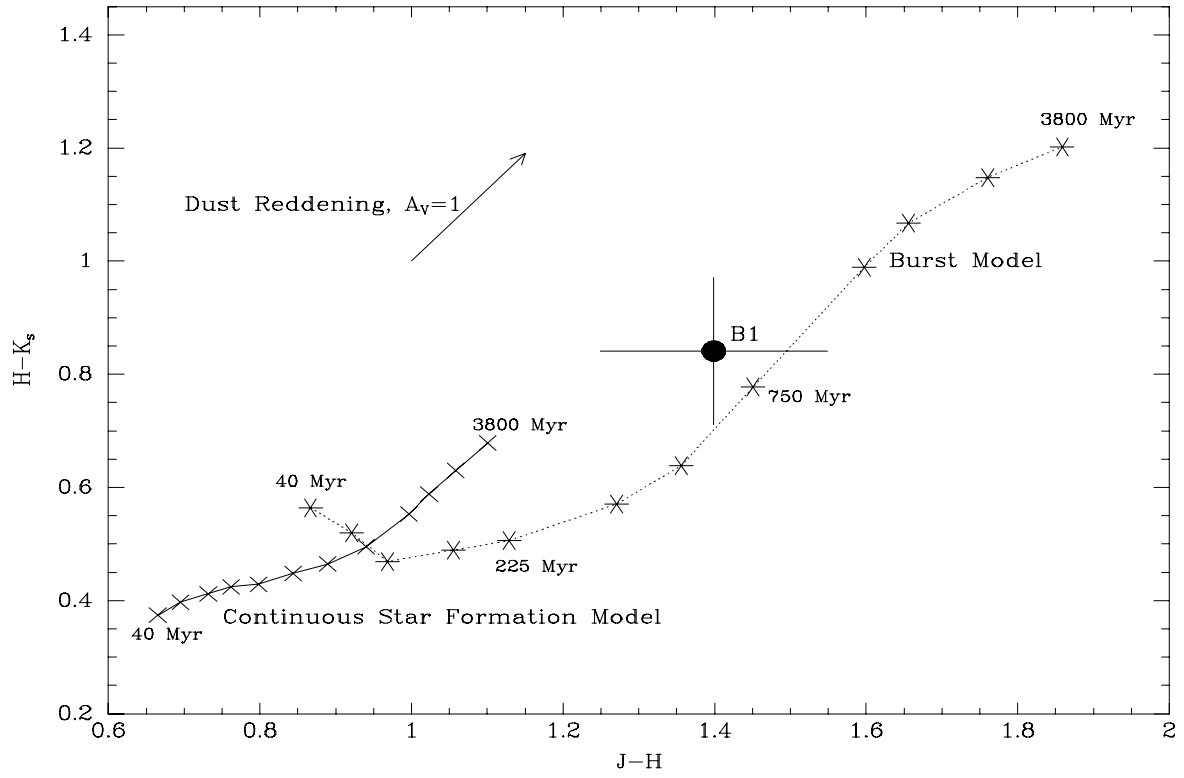


Fig. 6.— The integrated NTT  $J - H$  and  $H - K_s$  colors of B1. Model ages and extinction arrow as in Fig 5.



consider this to be a problem: a star formation rate of only  $\sim 0.1M_{\odot}\text{yr}^{-1}$  will produce OB stars sufficient to produce the observed blue flux.

- A dusty starburst model. The best fit is a model with a continuous star formation rate of  $\sim 10^3M_{\odot}\text{yr}^{-1}$ , an extinction of  $A_v = 2.3$  mag, and an age of 500 Myr. A slightly worse fit (but still acceptable at the  $2\sigma$  level) is younger (100 Myr), dustier ( $A_V = 3$  mag) and has a star formation rate of  $\sim 10^4M_{\odot}\text{yr}^{-1}$ .

The dusty starburst model is hard to reconcile with the strong Ly $\alpha$  emission of B1b, as Ly $\alpha$  is resonantly scattered and thus very strongly absorbed by even small amounts of dust.

B1c is much bluer, and can be fit either by an unreddened instantaneous burst model of age  $\sim 100$  Myr and mass  $\sim 3 \times 10^9M_{\odot}$ , or by a slightly dusty continuous star formation model, with a star formation rate of  $\sim 10M_{\odot}\text{yr}^{-1}$  and  $A_V \sim 1.0$ .

## 4.2. The Radial Profiles

In this section, we show that B1a and B1b are spatially extended. They are, however, very compact objects: too compact to be easily modelled as spiral galaxy disks. They appear to show colour gradients: bluer in their central regions.

In Figures 7 and 8 we compare the radial profiles of B1a and B1b with the relevant point spread functions (PSFs) measured from a bright star in the same image. B1a and B1b are marginally resolved in the F702W (rest-frame 2100 Å) and F110W (rest-frame 3250 Å) images. The F160W (rest-frame 4730Å) image was taken with NICMOS out of focus, and it does not significantly resolve B1a and B1b. The observed PSF does not vary significantly across the images, and is consistent with analytic predictions.

Although B1a and B1b are clearly resolved, both are very compact, with the observed surface brightness dropping to half its peak value within about  $0.1''$  ( $\sim 1$  kpc). This places a strong constraint on the size of the galaxies. Consider a disk galaxy, with a typical radial surface brightness profile of the form

$$I(r) = I_d \exp(-R/R_d)$$

(Binney & Merrifield 1998). The surface brightness of such a disk drops to half its peak value at  $r_{1/2} = 0.69R_d$  (Fig 9). Thus our observations require that  $R_d < 0.15'' \sim 1.2$  kpc. Only  $\sim 2\%$  of modern galaxy disks are this compact (Kent 1984). Now consider a spheroidal galaxy, with a radial surface brightness profile of the form

$$I(r) = I_e \exp\{-7.67[(R/R_e)^{1/4} - 1]\}$$

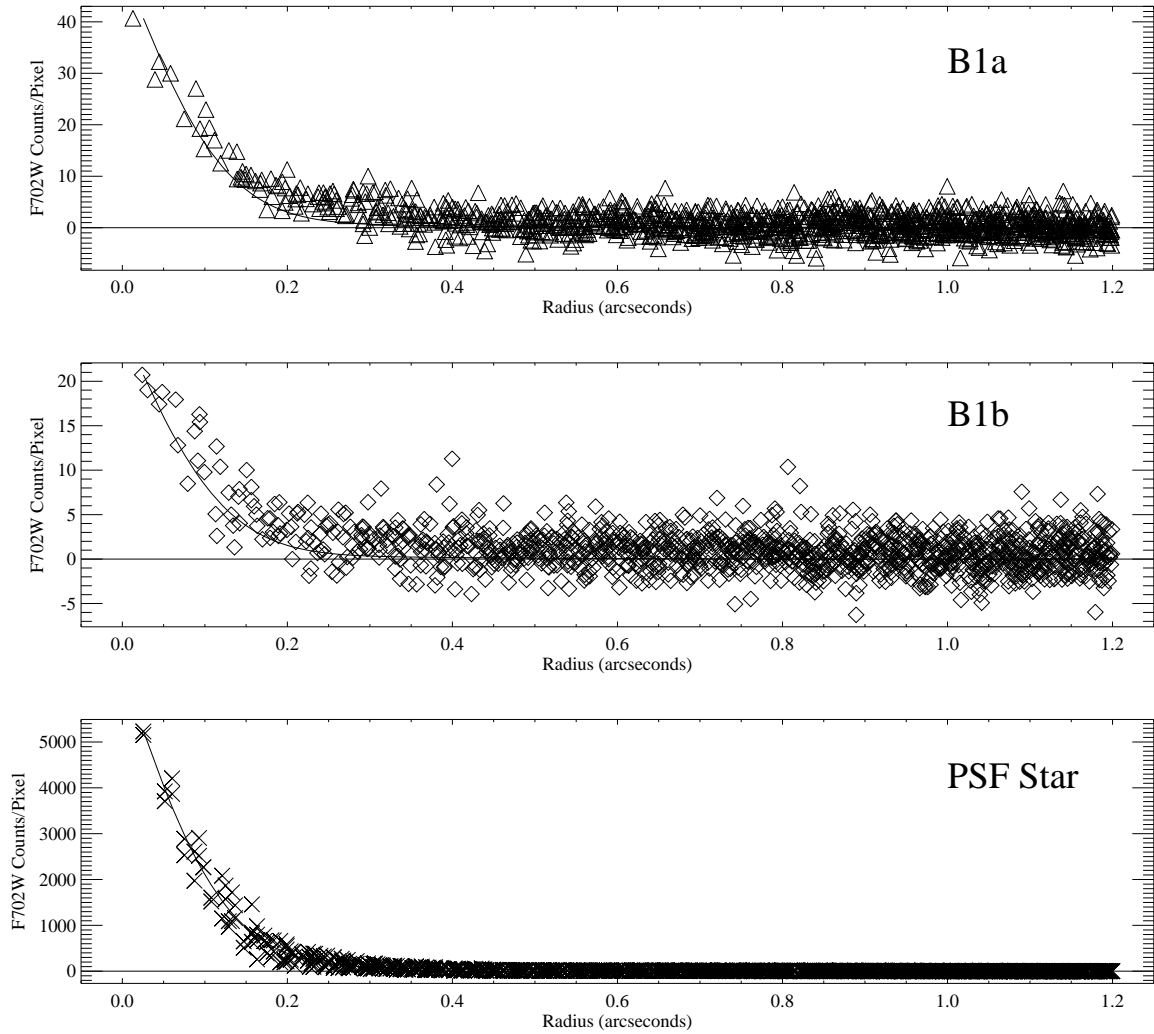


Fig. 7.— The F702W radial profiles of B1a, B1b and a point source image on the same chip. The solid line is an analytic fit to the PSF and is the same in all panels. The quadrant of each component that faces the other component has been excluded from the plots.

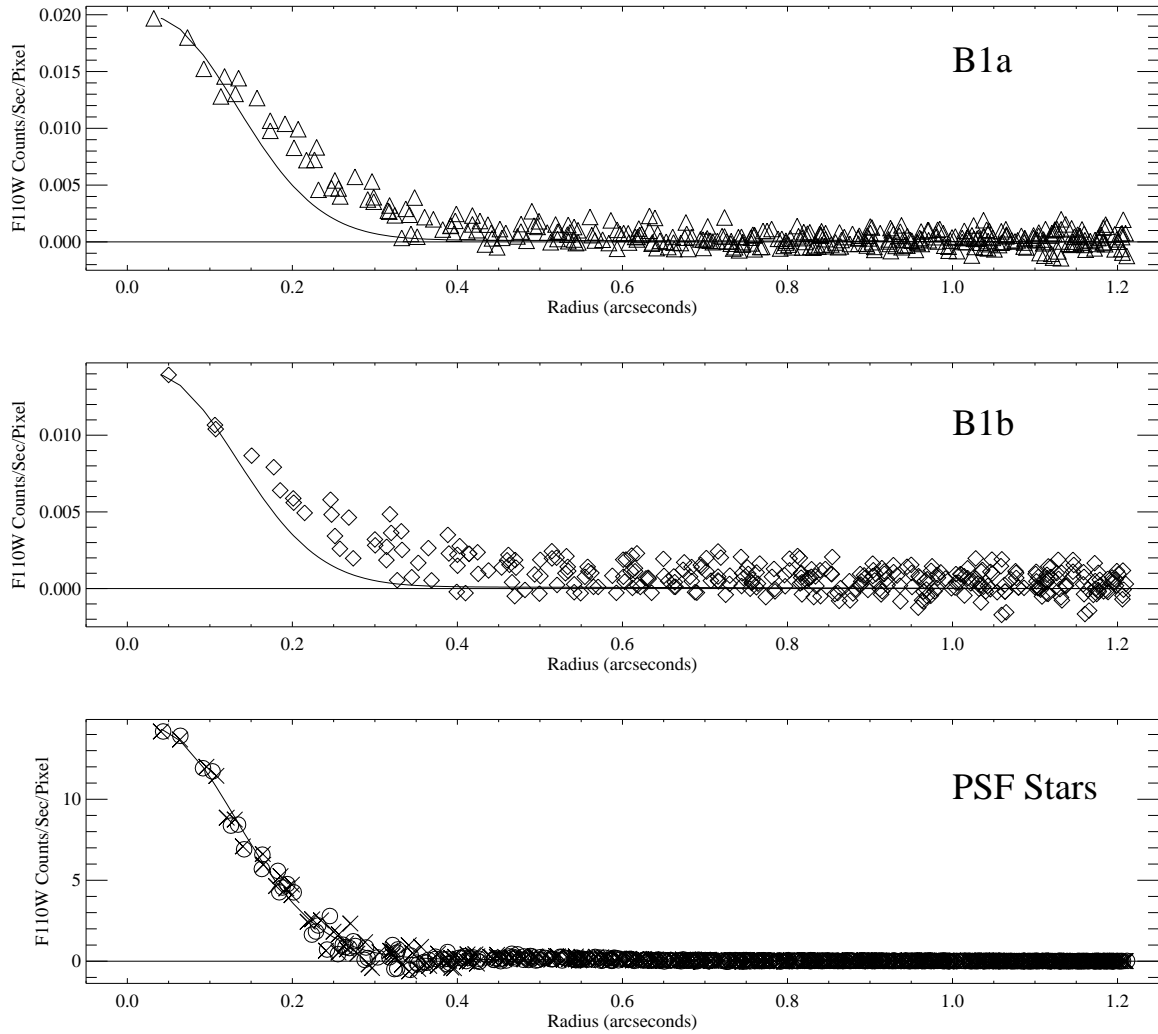


Fig. 8.— The F110W radial profiles of B1a, B1b and a point source from the same image. The solid line is an analytic fit to the PSF and is the same in all panels. The quadrant of each component that faces the other component has been excluded from the plots.

(Binney & Merrifield 1998). This profile is much more sharply peaked than the exponential disk profile, and its surface brightness drops to half its peak value at  $r_{1/2} = 0.13R_e$  (Fig 9). Thus  $R_e < 0.75'' \sim 6$  kpc. Over 50% of modern elliptical galaxies have effective radii this small (Djorgovski & Davis 1987).

More detailed modelling confirms these results. A wide variety of model galaxy profiles were convolved with PSFs and fit by  $\chi^2$  minimisation to the observed radial profiles. The modelling confirms that B1a and B1b are significantly extended. Both exponential disk models and spheroidal (de Vaucouleurs) models give acceptable fits to the data, as do models with a point source embedded in a fainter halo. Pure exponential disk models only give acceptable fits if  $R_d < 0.1''$  ( $\sim 800$  pc), which would place B1a and B1b in the most compact 1% of present-day disk galaxies. Spheroidal models give best fits for effective (half-light) radii  $R_e$  of around  $0.5''$  ( $\sim 4$  kpc), which are typical of modern elliptical galaxies. Models which combine a nuclear spheroid or point source with a disk can give acceptable fits, but only if the disk is unusually small and/or contributes only a small fraction ( $< 10\%$ ) of the light.

The compact radial profiles of B1a and B1b are typical of those of high redshift Lyman-break galaxies (Giavalisco, Steidel & Macchetto 1996). The inferred surface brightnesses in the rest-frame UV are comparable to those of faint Lyman-break galaxies, but the rest-frame optical surface brightnesses are an order of magnitude higher. As Giavalisco, Steidel & Macchetto (1996) note, these compact radial profiles are consistent with present-day elliptical galaxy profiles or bulges, but are much more compact than present-day disks.

Curiously, both B1a and B1b appear to be significantly larger at longer wavelengths. This can be seen in Figures 7 and 8: despite the wider PSF for the F110W filter, both components are clearly more extended than as seen through the F702W filter. Our modelling confirms this result: even after convolution with the relevant PSFs, no single model gives a good fit to either B1a or B1b at both F702W and F110W. The central  $\sim 1$  kpc of both components is  $\sim 0.3$  magnitudes bluer in F702W–F110W than the outer regions.

The change in size as a function of wavelength could be explained by a colour gradient within a single spheroidal component. It could also be explained by a two component model: a compact blue component that dominates at rest-frame  $2100\text{\AA}$  and a more diffuse (but still compact) red component that dominates at  $3250\text{\AA}$  and beyond. This red component, if disk-like, must have  $R_s < 0.2''$ , which would still place it in the most compact 1% of low redshift disks.

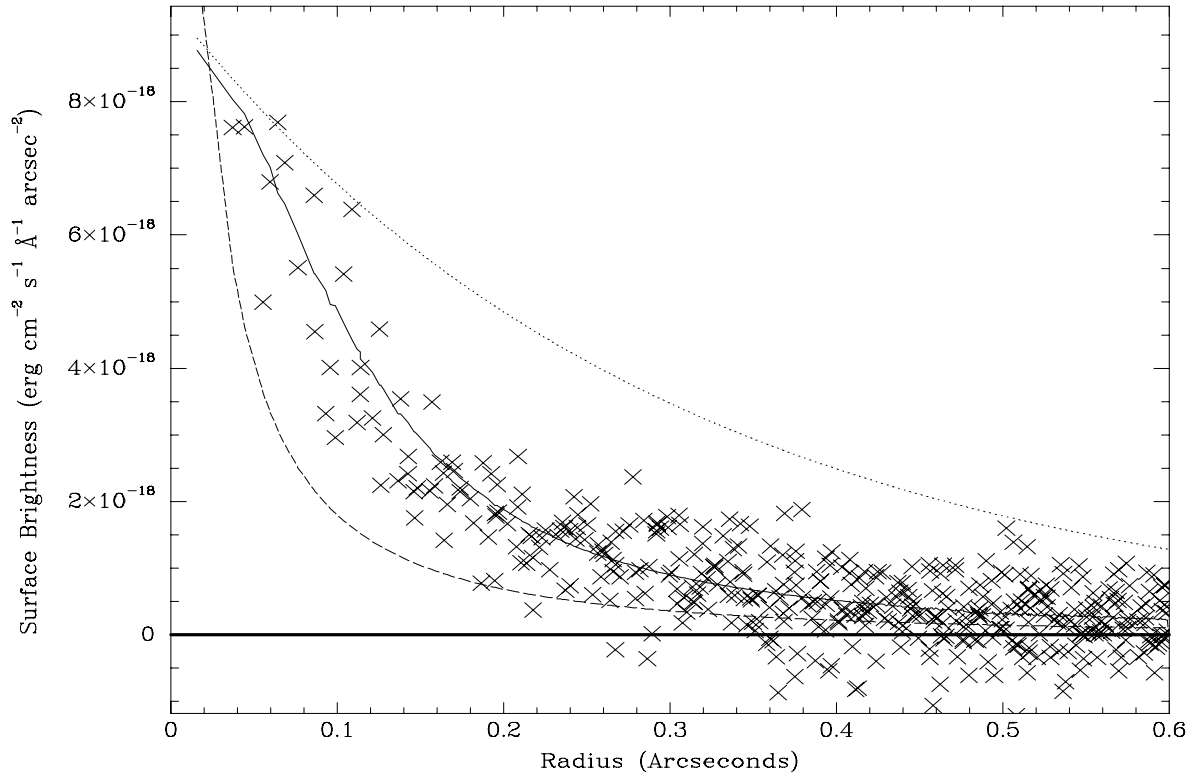


Fig. 9.— The F702W radial profile of B1a. The dashed curve (left) is a model spheroid with  $R_e = 0.5''$ . The dotted line (right) is a model disk with  $R_d = 0.3''$ . Both radii are typical of redshift zero galaxies. Neither model has been convolved with the PSF. The solid line is a spheroid with  $R_e = 0.5''$ , convolved with the PSF and scaled to fit.

### 4.3. Discussion

What are the continuum components of B1? B1c, with its blue colors, appears relatively straightforward: it is a region of extended moderate star formation, obscured by little dust. This star formation may be triggered by the interaction of B1a and B1b.

The nature of B1a and B1b is less straightforward. We consider four models in turn.

#### 4.3.1. Elliptical Galaxies

Could B1a and B1b be young elliptical galaxies? This hypothesis fits the data well.

- The radial profiles of B1a and B1b are well fit with de Vaucouleurs profiles, and the inferred radii are typical of present-day elliptical galaxies.
- The red colors are most easily explained by a  $> 10^{11} M_{\odot}$  stellar population which completed its star formation about 750 Myr before we observe it. It would thus be similar to modern E+A galaxies.
- B1 lies in an overdense region of the early universe (Francis, Wilson & Woodgate 2000), which may be the ancestor of a galaxy cluster.
- The velocity field around B1, if virial, implies masses of  $\sim 10^{12} M_{\odot}$ .

If B1a and B1b are elliptical galaxies, how do their surface brightnesses and sizes fit on the Kormendy relation (Kormendy 1977; Hoessel, Oegerle & Schneider 1987)? The F160W filter corresponds quite closely to the rest-frame  $B$ -band. The radial profile fitting suggests that both components have effective radii in the observed-frame near-IR of  $\sim 4$  kpc. Integrating a de Vaucouleurs profile over our photometric aperture, we can convert our observed  $F160W$  magnitudes into rest-frame  $B$ -band surface brightnesses at the effective radius. Were these components at low redshift, their surface brightnesses at the effective radius would be  $B_{0V} \sim 19.6$  mag arcsec $^{-2}$ . This is roughly an order of magnitude higher than the Kormendy relation would predict for an elliptical galaxy of this radius. This is consistent with passive evolution from our unreddened burst model (Section 4.1).

If B1a and B1b are elliptical galaxies, why do they apparently show color gradients? The UV emission from the central  $\sim 1$  kpc could be caused by a starburst, a hole in the dust or (for B1b) an AGN. Alternatively, some chemodynamical models predict color gradients in young elliptical galaxies (eg. Friaça & Terlevich 1998; Jiminez et al. 1999).

#### 4.3.2. *Dusty AGN*

A dusty AGN can certainly have colors as red as B1a and B1b (eg. Francis, Whiting and Webster 2000). The red components of B1a and B1b are however spatially extended, and hence cannot be produced by an AGN. Could the observed color gradient, however, be caused by the superposition of a compact blue AGN on a more extended, lower surface brightness red galaxy?

Even in the relatively blue central regions, the continuum slope is redder than  $F_\nu \propto \nu^{-2}$ , while radio-quiet QSOs have typical continuum slopes of  $F_\nu \propto \nu^{-0.5}$  (Francis, Whiting and Webster 2000). Any central AGN would thus have to be reddened by dust with  $E(B - V) > 0.2$ . This would make it hard for the Ly $\alpha$  emission from B1b to escape. In addition, the AGN in B1a and B1b would need remarkably equal luminosities and dust extinctions to explain the very similar observed colors and radial profiles of the two components. This fine tuning seems implausible. Furthermore, the high measured surface brightness was measured in the F160W band, to which the central blue component does not significantly contribute. We therefore conclude that while AGN may be present, they are unlikely to be responsible for the observed colors. Sensitive hard X-ray or far-IR observations will be required to determine whether a dusty AGN is present.

#### 4.3.3. *Dusty Disk Galaxies*

The more extended red component of B1a and B1b can be fit by a very compact exponential disk. Could these two objects then be compact spiral galaxies? The more compact bluer central component could be caused by AGNs or nuclear starbursts.

With sufficient dust, a spiral galaxy can certainly appear as red as these two components (Section 4.1.1). Two lines of reasoning however oppose this hypothesis.

1. Even the extended red components are extremely compact by the standards of modern disk galaxies. This could, however, be explained if disk galaxies form from the inside outwards.
2. This model requires that the outer (red) components of B1a and B1b be greatly reddened. This would make it difficult for the observed UV light and Ly $\alpha$  emission from the bluer central components to escape.

#### 4.3.4. *Bulges plus Low Surface Brightness Disks*

Could B1a and B1b be the bulges of two disk galaxies? The disks themselves may not have formed, or might be too low in surface brightness to be detected by the Hubble Space Telescope.

Two lines of reasoning oppose this hypothesis. Firstly, the red colors and  $H$ -band peak of B1 are seen in our ground-based photometry with large ( $\sim 5''$ ) apertures. Thus any extended component must have a similar stellar population to that inferred here. Secondly, the inferred masses and sizes for B1a and B1b are far larger than those typical of the bulges of disk galaxies.

## 5. The Ly $\alpha$ Nebula

B1 has a total Ly $\alpha$  luminosity of  $\sim 10^{44}$  erg s $^{-1}$ , spread over a region at least  $30 \times 100$  kpc in size. The emission consists of a number of diffuse, discrete components with relative velocities of  $\sim 700$  km s $^{-1}$ . What can produce such a luminous, diffuse, fast moving Ly $\alpha$  nebula?

The bulk motions of the Ly $\alpha$  nebula suggest that fast shocks must be present. We will show that such shocks are quite capable of producing the observed Ly $\alpha$  luminosity. The puzzle then becomes one of explaining the origins of the bulk motions.

It has also been suggested that photoionization by an AGN, or a cooling flow may power such nebulae. We discuss these possibilities, which are hard to exclude.

### 5.1. Physical Parameters of the Nebula

If we assume that the Ly $\alpha$  velocities are representative of the gas, and not an artifact of the high optical depth in Ly $\alpha$ , then the dynamical timescale (crossing time) of the nebula is  $\sim 10^8$  years. This is interestingly similar to the inferred age of the stellar population (Section 4.1).

What is the density of the nebula? The sight-line to background QSO 2139–4434 passes  $20''$  from B1 (though it does not pass through the Ly $\alpha$  nebula). The QSO spectrum shows a strong absorption-line system at the redshift of B1, with a column density  $N_H \sim 10^{19}$  (Francis, Wilson & Woodgate 2000). If we assume that the column density through the Ly $\alpha$  nebula is at least as great as this, and that the nebula is  $\sim 20$  kpc thick (ie. as thick



as it is wide) along the line of sight (both big assumptions), then its density must be at least  $10^{-4}\text{cm}^{-3}$ . If, however, the density were this low, the gas would be fully ionized by the metagalactic UV background at this redshift. If the nebula is  $\sim 20$  kpc thick, it must have a density of  $> 10^{-2}$  for its recombination rate to balance the photoionization from the UV background (Francis, Wilson & Woodgate 2000). The diffuse star formation of B1c, taking place within part of the Ly $\alpha$  nebula, also suggests that densities may be higher. In reality, of course, the cloud may be highly inhomogeneous, with dense neutral ‘bullets’ embedded in low density ionized gas.

If we take this lower limit on the density of the nebula ( $N_H > 10^{-2}\text{cm}^{-3}$ ), and assume that the nebula is 100 kpc long, 30 kpc wide and 10 kpc thick, then its hydrogen mass is  $\sim 10^{10}M_\odot$ .

## 5.2. Shock Models

Whenever there are blobs of gas moving at supersonic relative speeds, as are observed in the nebula, shocks are inevitable. We thus know that shocks are present. Could the emission from these shocks produce the observed Ly $\alpha$  emission?

### 5.2.1. Modelling

We used the fast shock models computed with the MAPPINGS III code to calculate the line emission from the shocks. MAPPINGS III is an updated version of the MAPPINGS II code (Dopita & Sutherland 1996) and uses improved radiation continuum and hydrogenic calculations to calculate the line and continuum radiation from shocks. The new version of the code enabled the calculation of a grid of shocks for a range of metallicities, up to 1000 km/s, although a small number of low metallicity models above 800 km s $^{-1}$  failed to converge after several global iterations. A fiducial model with a velocity of 700 km s $^{-1}$  was used here, having achieved a converged solution over a range of metallicities.

If the shocks are radiative, and if we assume, for example, a density of  $1\text{cm}^{-3}$ , then the Ly $\alpha$  emissivity will be  $0.13\text{erg cm}^{-2}\text{s}^{-1}$ , almost independent of the metallicity of the gas. A quarter of this comes from the shock itself, the rest coming from photoionization of the assumed neutral gas in front of the shock (the precursor region). If the shock is face-on to our sight-line, this would correspond to an observed surface brightness of  $1.6 \times 10^{-15}\text{erg cm}^{-2}\text{s}^{-1}\text{arcsec}^{-2}$ : nearly two orders of magnitude greater than the observed Ly $\alpha$  surface brightness (Section 3). Much of this may be self absorbed, but if even 1% escapes,

it can explain our observations. The predicted Ly $\alpha$ /C IV ratio is also consistent with the observations (Francis et al. 1996).

How does this vary with the assumed density of the gas? If the shocks are radiative, the emissivity will scale roughly with the density. Thus even with our lower limit on the density  $\rho = 10^{-2}\text{cm}^{-3}$  (Section 5), shocks can produce all the Ly $\alpha$  we observe.

Would these shocks be radiative? For our lower limit on the density,  $700\text{km s}^{-1}$  shocks become radiative on a timescale of  $\sim 10^8$  years, which is comparable to the dynamical timescale. Thus it seems likely that at least some fraction of the shocks will be radiative.

Thus shocks are probably present, and can easily produce the Ly $\alpha$  emission we observe. A number of factors could, however, suppress the Ly $\alpha$  emission from shocks.

1. The high optical depth in Ly $\alpha$  may have caused us to overestimate the velocity dispersion of the Ly $\alpha$  nebula. The emission from shocks is a strong function of their velocity:  $200\text{km s}^{-1}$  shocks emit two orders of magnitude less Ly $\alpha$  per unit area than our fiducial model.
2. The density of the Ly $\alpha$  nebula may be close to our lower limit of  $\rho = 10^{-2}\text{cm}^{-3}$ , in which case the Ly $\alpha$  emission, after the probable self absorption losses, could be an order of magnitude below the observed Ly $\alpha$  surface brightness.
3. The Ly $\alpha$  nebula could consist of small dense ‘bullets’ of neutral gas, moving at high speeds through a hot, highly ionized, low density medium. The bowshocks in the ionized medium would not be radiative, while the reverse shocks within the ‘bullets’ would be slow, and hence have low surface brightnesses (as well as having a small area).

### 5.2.2. *The Energy Source*

If the shock model is correct, the bulk gas motions explain the Ly $\alpha$  luminosity. What then could be the energy source for the bulk gas motions?

If we divide the total kinetic energy of the nebula (assuming a mass of  $\sim 10^{10}M_{\odot}$ ) by the Ly $\alpha$  luminosity, we can derive an upper limit on the damping time, which is  $\sim 10^7$  years. This is less than the dynamical timescale and stellar age of B1, suggesting that continued energy input is required. Note that the Ly $\alpha$  we observe may only be a small fraction of the Ly $\alpha$  emitted, which in turn will only be a small fraction ( $\sim 1\%$ ) of the total energy dissipation in the shocks. On the other hand, the gas mass may be greater than we are assuming.

If continued energy input is required, what can the source be? Perhaps the most natural energy source is the gravitational potential energy of B1. If we assume that B1 has a total mass of  $\sim 10^{12}M_{\odot}$ , then the gravitational potential energy released in its formation would be  $\sim 10^{61}$  ergs, which is more than sufficient to power the Ly $\alpha$  luminosity for the dynamical timescale. Such a mass for B1 would imply virial velocities in the Ly $\alpha$  nebula of  $\sim 500\text{km s}^{-1}$ , which are comparable to the bulk gas motions observed. This energy could be released by the merger of B1a and B1b, or by a continuing mass infall rate of  $\sim 10^3M_{\odot}\text{yr}^{-1}$ . Haiman, Spaans & Quataert (2000) point out that chemically primordial gas at a temperature of  $\sim 10^4$  K has few cooling mechanisms other than Ly $\alpha$  emission. Thus if most of the gas around B1 is primordial, a Ly $\alpha$  luminosity comparable to the gravitational binding energy (Section 5.2.2) of the system must be radiated.

Alternatively, Taniguchi & Shioya (2000) suggest that galactic superwinds driven by a starburst could power extended Ly $\alpha$  nebulae. This would naturally explain the similarity between the dynamical timescale and the inferred age of the stellar population in B1a and B1b. The maximum plausible amount of energy which star formation can inject into the intergalactic medium is  $\sim 10^{49}\text{erg } M_{\odot}^{-1}$  (eg. Bower et al. 2000). As B1a and B1b have a combined stellar mass of  $\sim 10^{11}M_{\odot}$ , the total energy liberated would be  $\sim 10^{60}$  ergs, which could in principle drive the observed Ly $\alpha$  luminosity for  $\sim 10^{10}$  years.

The Ly $\alpha$  emission in high redshift radio galaxies has sometimes been ascribed to mechanical energy deposition by a radio jet (eg. Bicknell et al. 2000). Could such a jet be present in B1? We do not detect any radio emission from B1 (Francis et al. 1996). Our  $3\sigma$  upper limit of 0.23 mJy at 2.4 GHz corresponds to a luminosity limit of  $10^{33}\text{ergs s}^{-1}\text{Hz}^{-1}$  at rest-frame 1.4 GHz (assuming a typical radio galaxy radio spectrum of the form  $F_{\nu} \propto \nu^{-0.8}$ ). Typical ratios of the total jet mechanical power to the monochromatic radio flux at 1.4 GHz are  $\sim 10^{11}\text{--}10^{12}\text{Hz}^{-1}$  (Bicknell et al. 1998). Thus we can place an upper limit of  $\sim 10^{45}\text{erg s}^{-1}$  on the energy injection from a radio jet. This is sufficient to power the observed Ly $\alpha$  luminosity only if  $> 10\%$  of the mechanical energy is converted into observable Ly $\alpha$  emission, which seems implausible. Deeper radio observations should test this hypothesis.

### 5.3. Other Models

If the shock emission is suppressed, is there an alternative mechanism capable of producing the Ly $\alpha$  emission?

Stellar ionisation (by hot young stars) is incapable of producing the observed C IV emission. Photoionisation by the UV continuum radiation from a QSO can, however, produce

both the Ly $\alpha$  and C IV, as discussed by Francis, Woodgate & Danks (1997). We do not see strong UV continuum emission from any component of B1, so such an AGN would have to be concealed from our sight-line. Chapman et al. (2000) detected strong sub-mm emission from a Ly $\alpha$  blob at  $z = 3.09$ , suggesting that a dusty AGN or starburst was present, but we have no evidence for such a source in B1.

Extended emission-line nebulosities are associated with many low redshift cooling flow clusters, such as NGC 1275. As all high-redshift Ly $\alpha$  blobs seem to lie in cluster environments, could the Ly $\alpha$  luminosity be associated with a cooling flow (eg. Fabian et al. 1986)?

Steidel et al. (2000) suggest that Ly $\alpha$  nebulae are caused by gas cooling from higher temperatures, in such a cooling flow. If each cooling hydrogen atom produces one Ly $\alpha$  photon, however, we require that  $\sim 10^6 M_{\odot} \text{yr}^{-1}$  of hydrogen be cooling onto B1. This would build the observed baryonic mass of B1 in  $< 10^5$  years. This is far smaller than either the dynamical time or the age of the stellar population in B1a and B1b, so the simple cooling model seems implausible.

Note that the nebular emission-line luminosities of low redshift cooling-flow clusters are also orders of magnitude too great to be explained by this simple recombination mechanism (eg. Voit & Donahue 1997). The cause of this discrepancy is still controversial even at low redshifts.

On purely energetic grounds, could the Ly $\alpha$  luminosity be powered by the thermal energy in the nebula? If we divide the thermal energy of  $10^{10} M_{\odot}$  of hydrogen at  $10^6$  K by the observed Ly $\alpha$  luminosity, we get a timescale of  $\sim 10^7$  years: shorter than the dynamical timescale or the stellar age.  $10^{10} M_{\odot}$  may however be an underestimate of the true gaseous mass of the Ly $\alpha$  nebula, particularly if the neutral gas we observe is immersed in a much more massive cloud of hot, highly ionised X-ray emitting gas.

## 6. Conclusions

So what is B1? On balance, we conclude that B1a and B1b are probably young elliptical galaxies, perhaps analogues of E+A galaxies today. Both their red colors and compact sizes are naturally explained by this model. An extremely dusty starburst in the central regions of a disk galaxy can however, with some fine tuning, reproduce the colors and sizes. The bluer colors of the centres of both components, and the Ly $\alpha$  emission from the core of B1b are, however, arguments against the presence of large amounts of dust in these systems. Near-IR H-band spectroscopy on an 8m-class telescope should resolve this ambiguity, by detecting the spectral signatures of a Balmer/4000Å break. B1c appears to be a region of relatively

unobscured star formation, perhaps induced by the interaction of B1a and B1b.

If B1a and B1b are elliptical galaxies, their surface brightnesses are an order of magnitude greater than those that the Kormendy relation would predict for galaxies of this size, and they show strong radial color gradients, with blue cores. The very existence of massive elliptical galaxies at this redshift, if confirmed, is interesting (eg. Treu & Stiavelli 1999, and references therein). These galaxies would give us a chance to study young elliptical galaxies for the first time. Our observations would pose several puzzles:

- Why is the surface brightness of these galaxies so great? Is this simply due to passive evolution?
- Why do both galaxies show strong, but very similar color gradients?
- Is the remarkable similarity and proximity of the two galaxies coincidental, or is it telling us something about how cluster elliptical galaxies form?
- If these galaxies are so massive and red at  $z = 2.38$ , what would they have looked like at  $z \sim 3$  when they were forming?

The nature of the Ly $\alpha$  nebula is less well constrained by our observations. The nebula could be excited by photoionization from an AGN, by whatever powers low redshift cooling flow nebulae, or by fast shocks powered by either superwinds or gravitational potential energy. Spatially resolved spectroscopy of other emission lines will help discriminate between these models.

We wish to thank Joss Bland-Hawthorn and Catherine Drake for their assistance at with the TTF observations, and all the staff at CTIO for heroic efforts to get the mosaic camera working for us. We are grateful to Mike Dopita, Megan Donahue and Martijn de Kool and Ian George for helpful discussions. Hsiao-Wen Chen was instrumental in getting the slitless STIS spectrum extraction software working. David Hogg’s cosmology crib sheet (astro-ph/9905116) was very helpful to us.

## REFERENCES

- Adelberger, K.L. & Steidel, C.C. 2000, ApJ, 544, 218
- Bertin, E. & Arnouts, S. 1996, A&AS, 117, 393

- Bicknell, G.V., Dopita, M.A., Tsvetanov, Z.I., & Sutherland, R.S. 1998, *ApJ*, 495, 680
- Bicknell, G.V., Sutherland, R.S., van Breughel, W.J.M., Dopita, M.A., Dey, A. & Miley, G.K. 2000, *ApJ*, submitted.
- Binette, L., Wang, J.C.L., Zuo, L., & Magris, C.G. 1993, *AJ*, 105, 797
- Binney, J. & Merrifield, M. 1998, *Galactic Astronomy*, Princeton University Press, (Princeton NJ)
- Bland-Hawthorn, J. & Heath-Jones, D. 1998, *PASA*, 15, 44
- Bower, R.G., Benson, A.J., Baugh, C.M., Cole, S., Frenk, C.S. & Lacey, C.G. 2000, *MNRAS*, submitted (astro-ph/0006109)
- Bruzual, A. G., & Charlot, S. 1993, *ApJ*, 405, 538
- Calzetti, D., Kinney, A. L., & Storchi-Bergmann, T. 1994, *ApJ*, 429, 582
- Cardelli, J.A., Clayton, G.C. & Mathis, J.S. 1989, *ApJ*, 345, 245
- Carilli, C.L., Röttgering, H.J.A., van Ojik, R., Miley, G.K. & van Breughel, W.J.M. 1997, *ApJS*, 109, 1
- Carter, B. S., & Meadows, V. S. 1995, *MNRAS*, 276, 734
- Chapman, S.C., Lewis, G.F., Scott, D., Richards, E., Borys, C., Steidel, C.C., Adelberger, K.L. & Shapley, A.E. 2000, *ApJ* in press (astro-ph/0010101)
- Chen, H.-W., Lanzetta, K.M., & Pascarella, S. 1999, *Nature*, 398, 586
- Cimatti, A., Daddi, E., di Serego Alighieri, S., Pozzetti, L., Mannucci, F., Renzini, A., Oliva, E., Zamorani, G., Andreani, P. & Röttgering, H.J.A. 1999, *A&A*, 352, 45
- Djorgovski, S. & Davis, M. 1987, *ApJ*, 313, 59
- Dopita, M.A. & Sutherland, R.S. 1996, *ApJS*, 102, 161
- Dunlop, J., Peacock, J.A., Spinrad, H.J., Dey, A., Jiminez, R., Stern, D. & Windhorst, R. 1996, *Nature*, 381, 581
- Eales, S., Rawlings, S., Puxley, P., Rocca-Volmerange, B. & Kuntz, K. 1993, *Nature*, 363, 140
- Fabian, A.C., Arnaud, K.A., Nulsen, P.E.J., & Mushotsky, R.F. 1986, *ApJ*, 305, 9

- Francis, P.J., Hewett, P.C., Foltz, C.B., Chaffee, F.H., Weymann, R.J. & Morris, S.L. 1991, ApJ, 373, 465
- Francis, P. J., & Hewett, P. C. 1993, AJ, 105, 1633
- Francis, P. J., et al. 1996, ApJ, 457, 490
- Francis, P.J., Whiting, M.T.& Webster, R.L. 2000, PASA, 17, 56
- Francis, P.J., Wilson, G.M. & Woodgate, B.E. 2000, PASA in press.
- Francis, P. J., Woodgate, B. E. & Danks, A. C., 1997, ApJ, 482, 25
- Friça, A.C.S. & Terlevich, R.J. 1998, MNRAS, 298, 399
- Fruchter, A.S. & Hook, R.N. 1998, PASP, submitted (astro-ph/9808087)
- Gardner, J.P. et al. 1998, ApJ, 492, L99
- Giavalisco, M., Steidel, C.C. & Macchetto, F.D. 1996, ApJ, 470, 189
- Haiman, Z., Spaans, M. & Quataert, E. 2000, ApJ, 537, L5
- Hoessel, J.G., Oegerle, W.R. & Schneider, D.P. 1994, AJ, 94, 1111
- Hu, E.M., Cowie, L. L., & McMahon, R. G. 1998, ApJ, 502, L99
- Hu, E.M., & Ridgway, S. 1994, AJ, 107, 156
- Hughes, D. et al. 1998, Nature, 394, 241
- Iverson, R.J., Dunlop, J.S., Smail, I., Dey, A., Liu, M.C. & Graham, J.R. 2000, ApJ, in press (astro-ph/0005234)
- Jimenez, R., Friça, A.C.S., Dunlop, J.S., Terlevich, R.J., Peacock, J.A. & Nolan, L.A. 1999, MNRAS, 305, L16
- Keel, W.C., Cohen, S.H., Windhorst, R.A. & Waddington, I. 1999, AJ, 118, 2547
- Kennicutt, R.C. 1983, ApJ, 272, 54
- Kennicutt, R.C. 1992, ApJ, 388, 310
- Kent, S.M, 1984, ApJS, 56, 105
- Kobulnicky, H.A. & Koo, D. 2000, ApJ, in press (astro-ph/0008242)

- Kormendy, J. 1977, *ApJ*, 214, 359
- Kudritzki, R.-P., Méndez, R.P., Feldmeier, J.J., Ciardullo, R., Jacoby, G.H., Freeman, K.C., Arnaboldi, M., Capaccioli, M., Gerhard, O. & Ford, H.C. 2000, *ApJ*, in press (astro-ph/0001156)
- Lidman, C., Cuby, J.-G. & Vanzi, L. 2000, “SOFI users manual”, Version 1.3 (Garching: ESO)
- Lindler, D. 1998, CALSTIS Reference Guide Version 5.1), <http://hires.gsfc.nasa.gov/stis/software/software.html>
- Lindler, D. 2000, personal communication.
- Lowenthal, J. D., Hogan, C. J., Green, R. F., Caulet, A., Woodgate, B. E., Brown, L., & Foltz, C. B. 1991, *ApJ*, 377, L73
- Lowenthal, J.D., Hogan, C.J., Green, R.F., Caulet, A., Woodgate, B.E., Brown, L. & Foltz, C.B. 1991, *ApJ*, 377, L73
- McCarthy, P.J. 1993, *ARA&A*, 31, 639
- McLeod, B.A. 1997, in “HST Calibration Workshop”, eds Casertano, S., Jedrzejewski, R., Keyes, C.D. & Stevens, M. (STScI, Baltimore)
- Moriondo, G., Cimatti, A. & Daddi, E. 2000, *A&A*, in press (astro-ph/0010335)
- Muller, G.P., Reed, R., Armandroff, T., Boroson, T.A. & Jacoby, G.H. 1998, *Proc SPIE*, 3355, 577
- Osterbrock, D. E. & Martel, A. 1993, *ApJ*, 414, 552
- Pascarelle, S.M., Windhorst, R.A., Driver, S.M. & Ostrander, E.J. 1996, *ApJ*, 456, L21
- Pascarelle, S.M., Windhorst, R.A. & Keel, W.C. 1998, *AJ*, 116, 2659
- Persson, S.E., Murphy, D.C., Krzeminski, W., Roth, M. & Rieke, M.J. 1998, *AJ*, 116, 2475
- Pentericci, L., Röttgering, H.J.A., Miley, G.K., Carilli, C.L. & McCarthy, P. 1997, *A&A*, 326, 580
- Roche, N., Lowenthal, J. & Woodgate, B. 2000, *ApJ*, submitted (astro-ph/0002160)
- Schlegel, D.J., Finkbeiner, D.P. & David, M. 1998, *ApJ*, 500, 525



- Smail, I., Ivison, R.J., Kneib, J.-P., Cowie, L.L., Blain, A.W., Barger, A.J., Owen, F.N., & Morrison, G. 1999, MNRAS in press (astro-ph/9905246)
- Soifer, B.T., Matthews, K., Neugebauer, G., Armus, L. Cohen, J.G. & Persson, S.E. 1999, AJ, 118, 2065
- Steidel, C. C., Giavalisco, M., Pettini, M., Dickinson, M. & Adelberger, K. L. 1996, ApJ, 462, L17
- Steidel, C.C., Adelberger, K.L., Shapley, A.E., Pettini, M. Dickinson, M. & Giavalisco, G. 2000, ApJ, 532, 170
- Taniguchi, Y. & Shioya, Y. 2000, ApJ, 532, L13
- Teplitz, H.I. et al. 2000, ApJ, 533, 65
- Thompson, D. et al. 1999, ApJ, 523, 100
- Thompson, R.I., Rieke, M., Schneider, G., Hines, D.C. & Corbin, M.R. 1998, ApJ, 492, L95
- Trauger, J.T. et al. ApJ, 435, 3
- Treu, T. & Stiavelli, M. 1999, ApJ, 524, 27
- Voges, W. et al. 1999, A&A, 349, 389
- Voit, G.M. & Donahue, M. 1997, ApJ, 486, 242
- Woodgate, B.E. et al. 1998, PASP, 110, 1183
- Wynne, L.G. & Worswick, S.P. 1988, The Observatory, 108, 161